Spectral engineering by Gaussian phase-matching for quantum photonics

P. Ben Dixon, * **Jeffrey H. Shapiro, and Franco N. C. Wong**

Research Laboratory of Electronics, Massachusetts Institute of Technology, Cambridge, MA 02139, USA

*bendixon@mit.edu

Abstract: We demonstrate Gaussian-shaped phase matching of a periodically-poled potassium titanyl phosphate (PPKTP) crystal by imposing a custom duty-cycle pattern on its grating structure while keeping the grating period fixed. The PPKTP's phase-matching characteristics are verified through optical difference-frequency generation measurements, showing good agreement with expected values based on our design parameters. Our theoretical analysis predicts that under extended phase-matching conditions the custom-poled PPKTP crystal is capable of generating heralded single photons with a spectral purity of 97%, and can reach as high as 99.5% with gentle spectral filtering, something that is highly desirable for photonic quantum information processing applications.

OCIS codes: (270.5585) Quantum information and processing; (190.4410) Nonlinear optics, parametric processes.

References and links

1. P. Kok, H. Lee, and J. P. Dowling, "Creation of large-photon-number path entanglement conditioned on photodetection," Phys. Rev. A **65,** 052104 (2002).
2. T. Nagata, R. Okamoto, J. L. O'Brien, K. Sasaki, and S. Takeuchi, "Beating the standard quantum limit with four-entangled photons," Science **316,** 726–729 (2007).
3. V. Giovannetti, S. Lloyd, and L. Maccone, "Quantum-enhanced measurements: Beating the standard quantum limit," Science **306,** 1330–1336 (2004).
4. M. Halder, A. Beveratos, N. Gisin, V. Scarani, C. Simon, and H. Zbinden, "Entangling independent photons by time measurement," Nat. Phys. **3,** 692–695 (2007).
5. R. Kaltenbaek, R. Prevedel, M. Aspelmeyer, and A. Zeilinger, "High-fidelity entanglement swapping with fully independent sources," Phys. Rev. A **79,** 040302 (2009).
6. S. Aaronson and A. Arkhipov, "The computational complexity of linear optics," arXiv:1011.3245 [quant-ph] (2010).
7. A. Aspuru-Guzik and P. Walther, "Photonic quantum simulators," Nat. Phys. **8,** 285–291 (2012).
8. T. Peyronel, O. Firstenberg, Q.-Y. Liang, S. Hoffenberth, A. V. Gorshkov, T. Pohl, M. D. Lukin, and V. Vuletić, "Quantum nonlinear optics with single photons enabled by strongly interacting atoms," Nature **488,** 57–60 (2012).
9. A. Muller, W. Fang, J. Lawall, and G. S. Solomon, "Creating polarization-entangled photon pairs from a semiconductor quantum dot using the optical stark effect," Phys. Rev. Lett. **103,** 217402 (2009).
10. J. Chen, K. F. Lee, C. Liang, and P. Kumar, "Fiber-based telecom-band degenerate-frequency source of entangled photon pairs," Opt. Lett. **31,** 2798–2800 (2006).
11. C. K. Hong and L. Mandel, "Theory of parametric frequency down conversion of light," Phys. Rev. A **31,** 2409–2418 (1985).
12. C. Gerry and P. Knight, *Introductory Quantum Optics* (Cambridge University Press, 2004).
13. P. J. Mosley, J. S. Lundeen, B. J. Smith, P. Wasylczyk, A. B. U'Ren, C. Silberhorn, and I. A. Walmsley, "Heralded generation of ultrafast single photons in pure quantum states," Phys. Rev. Lett. **100,** 133601 (2008).
14. A. B. U'Ren, C. Silberhorn, R. Erdmann, K. Banaszek, W. P. Grice, I. A. Walmsley, and M. G. Raymer, "Generation of pure-state single-photon wavepackets by conditional preparation based on spontaneous parametric downconversion," Las. Phys. **15,** 146 (2005).

#182231 - $15.00 USD Received 21 Dec 2012; revised 21 Feb 2013; accepted 21 Feb 2013; published 1 Mar 2013

15. C. K. Hong, Z. Y. Ou, and L. Mandel, "Measurement of subpicosecond time intervals between two photons by interference," Phys. Rev. Lett. **59,** 2044–2046 (1987).
16. R. Kaltenbaek, B. Blauensteiner, M. Żukowski, M. Aspelmeyer, and A. Zeilinger, "Experimental interference of independent photons," Phys. Rev. Lett. **96,** 240502 (2006).
17. W. P. Grice, A. B. U'Ren, and I. A. Walmsley, "Eliminating frequency and space-time correlations in multiphoton states," Phys. Rev. A **64,** 063815 (2001).
18. O. Kuzucu, F. N. C. Wong, S. Kurimura, and S. Tovstonog, "Joint temporal density measurements for two-photon state characterization," Phys. Rev. Lett. **101,** 153602 (2008).
19. O. Cohen, J. S. Lundeen, B. J. Smith, G. Puentes, P. J. Mosley, and I. A. Walmsley, "Tailored photon-pair generation in optical fibers," Phys. Rev. Lett. **102,** 123603 (2009).
20. R. Rangarajan, L. E. Vicent, A. B. U'Ren, and P. G. Kwiat, "Engineering an ideal indistinguishable photon-pair source for optical quantum information processing," J. Mod. Opt. **58,** 318–327 (2011).
21. A. M. Brańczyk, A. Fedrizzi, T. M. Stace, T. C. Ralph, and A. G. White, "Engineered optical nonlinearity for quantum light sources," Opt. Express **19,** 55–65 (2011).
22. T. Gerrits, M. J. Stevens, B. Baek, B. Calkins, A. Lita, S. Glancy, E. Knill, S. W. Nam, R. P. Mirin, R. H. Hadfield, R. S. Bennink, W. P. Grice, S. Dorenbos, T. Zijlstra, T. Klapwijk, and V. Zwiller, "Generation of degenerate, factorizable, pulsed squeezed light at telecom wavelengths," Opt. Express **19,** 24434–24447 (2011).
23. E. Pomarico, B. Sanguinetti, C. I. Osorio, H. Herrmann, and R. T. Thew, "Engineering integrated pure narrowband photon sources," New J. Phys. **14,** 033008 (2012).
24. I. Ali Khan and J. C. Howell, "Experimental demonstration of high two-photon time-energy entanglement," Phys. Rev. A **73,** 031801 (2006).
25. Y.-P. Huang, J. B. Altepeter, and P. Kumar, "Heralding single photons without spectral factorability," Phys. Rev. A **82,** 043826 (2010).
26. R. S. Bennink, "Optimal collinear Gaussian beams for spontaneous parametric down-conversion," Phys. Rev. A **81,** 053805 (2010).
27. C. K. Law, I. A. Walmsley, and J. H. Eberly, "Continuous frequency entanglement: Effective finite Hilbert space and entropy control," Phys. Rev. Lett. **84,** 5304–5307 (2000).
28. C. K. Law and J. H. Eberly, "Analysis and interpretation of high transverse entanglement in optical parametric down conversion," Phys. Rev. Lett. **92,** 127903 (2004).
29. R. Erdmann, D. Branning, W. Grice, and I. A. Walmsley, "Restoring dispersion cancellation for entangled photons produced by ultrashort pulses," Phys. Rev. A **62,** 053810 (2000).
30. V. Giovannetti, L. Maccone, J. H. Shapiro, and F. N. C. Wong, "Generating entangled two-photon states with coincident frequencies," Phys. Rev. Lett. **88,** 183602 (2002).
31. O. Kuzucu, M. Fiorentino, M. A. Albota, F. N. C. Wong, and F. X. Kärtner, "Two-Photon Coincident-Frequency Entanglement via Extended Phase Matching," Phys. Rev. Lett. **94,** 083601 (2005).
32. V. Giovannetti, L. Maccone, J. H. Shapiro, and F. N. C. Wong, "Extended phase-matching conditions for improved entanglement generation," Phys. Rev. A **66,** 043813 (2002).
33. P. J. Mosley, J. S. Lundeen, B. J. Smith, and I. A. Walmsley, "Conditional preparation of single photons using parametric downconversion: a recipe for purity," New J. Phys. **10,** 093011 (2008).
34. A. Christ, A. Eckstein, P. J. Mosley, and C. Silberhorn, "Pure single photon generation by type-I PDC with backward-wave amplification," Opt. Express **17,** 3441–3446 (2009).
35. M. G. Raymer, J. Noh, K. Banaszek, and I. A. Walmsley, "Pure-state single-photon wave-packet generation by parametric down-conversion in a distributed microcavity," Phys. Rev. A **72,** 023825 (2005).
36. R. Boyd, *Nonlinear Optics* (Academic Press, 1992).
37. M. Fejer, G. Magel, D. Jundt, and R. Byer, "Quasi-phase-matched second harmonic generation: tuning and tolerances," IEEE J. Quant.Electron. **28,** 2631–2654 (1992).
38. M. A. Arbore, A. Galvanauskas, D. Harter, M. H. Chou, and M. M. Fejer, "Engineerable compression of ultrashort pulses by use of second-harmonic generation in chirped-period-poled lithium niobate," Opt. Lett. **22,** 1341–1343 (1997).
39. M. B. Nasr, S. Carrasco, B. E. A. Saleh, A. V. Sergienko, M. C. Teich, J. P. Torres, L. Torner, D. S. Hum, and M. M. Fejer, "Ultrabroadband biphotons generated via chirped quasi-phase-matched optical parametric down-conversion," Phys. Rev. Lett. **100,** 183601 (2008).
40. T. Y. Fan, C. E. Huang, B. Q. Hu, R. C. Eckardt, Y. X. Fan, R. L. Byer, and R. S. Feigelson, "Second harmonic generation and accurate index of refraction measurements in flux-grown $KTiOPO_4$," Appl. Opt. **26,** 2390–2394 (1987).
41. D. H. Jundt, "Temperature-dependent Sellmeier equation for the index of refraction, n_e, in congruent lithium niobate," Opt. Lett. **22,** 1553–1555 (1997).
42. K. Fradkin, A. Arie, A. Skliar, and G. Rosenman, "Tunable midinfrared source by difference frequency generation in bulk periodically poled $KTiOPO_4$," Appl. Phys. Lett. **74,** 914–916 (1999).
43. F. König and F. N. C. Wong, "Extended phase matching of second-harmonic generation in periodically poled $KTiOPO_4$ with zero group-velocity mismatch," Appl. Phys. Lett. **84,** 1644–1646 (2004).
44. S. Popescu and D. Rohrlich, "Thermodynamics and the measure of entanglement," Phys. Rev. A **56,** R3319–

#182231 - $15.00 USD Received 21 Dec 2012; revised 21 Feb 2013; accepted 21 Feb 2013; published 1 Mar 2013

R3321 (1997).
45. O. Kuzucu, F. N. C. Wong, S. Kurimura, and S. Tovstonog, "Time-resolved single-photon detection by femtosecond upconversion," Opt. Lett. **33,** 2257–2259 (2008).

1. Introduction

The ability to generate and shape non-classical states of light is an essential part of any quantum information processing toolbox for quantum computation, measurement, and communication. Applications that benefit from better enabling technologies in quantum photonics include, for example, multi-photon precision measurements [1–3], high fidelity quantum repeaters for use in long-distance quantum communication [4, 5], quantum computation [6] and quantum simulations [7].

There are several ways to generate single and entangled photons, including atomic ensembles [8], quantum dots [9], and optical fibers [10]. The most commonly used sources, however, employ nonlinear optical crystals—such as beta-barium borate (BBO) or periodically-poled potassium titanyl phosphate (PPKTP)—through the process of spontaneous parametric down-conversion (SPDC) [11, 12]. SPDC sources create two-photon states (biphotons) that, under appropriate conditions, can be used to create a particularly desirable quantum state: a heralded spectrally-pure single photon [13, 14].

Many applications, such as measurement-based linear optics quantum computation, utilize Hong-Ou-Mandel (HOM) type quantum interactions [15] between two independent photons, and thus require the simultaneous arrival of two or more spectrally identical photons [16]. This indistinguishability can be achieved with single photons in a single spectral mode (or equivalently a single temporal mode), hence generating these single-mode photons has been the focus of many recent studies [13, 14, 17–23].

To generate pure-state single photons from SPDC one needs to perform two tasks: heralding single photons and ensuring their spectral purity. Heralding single photons is relatively easy: when one photon of a photon pair generated by SPDC is detected, it heralds the presence of the conjugate photon from the pair. Ensuring spectral purity is not so simple: SPDC biphotons can possess strong spectral correlations [24], such that the detection of one photon renders the conjugate photon to be in a mixed state of all its possible spectral components. This yields single photons with low spectral purity (and correspondingly high temporal uncertainty).

Different techniques can be used to increase the spectral purity of single photons, all involving some kind of spectral engineering of the generation or detection process. An obvious method is to spectrally filter the heralding photon using a narrow-band filter, reducing the heralded photon to one or very few spectral modes. This works reasonably well, at the expense of severely reducing the flux of the heralded photons, which limits their usefulness in practical applications [16]. Temporal filtering has also been suggested [25], taking advantage of detector measurement response times to approximate single-spatiotemporal-mode operation. Additionally, spatial-mode selection by optimizing pump focusing and collection optics for SPDC outputs from bulk nonlinear crystals is also necessary to achieve high spectral purity and high heralding efficiency [26].

To achieve high spectral decorrelation it is necessary to understand spectral entanglement of SPDC in terms of its biphoton output state's Schmidt decomposition [27], and how various parameters affect the Schmidt number [28] of that state (a Schmidt number of 1 corresponds to a separable state). Spectral engineering refers to methods for manipulating the amount of spectral entanglement by choosing appropriate combinations of pump and crystal properties, such as pump bandwidth, crystal length, and grating structures for periodically-poled materials. Specifically, it is of interest to remove all spectral entanglement for SPDC biphotons to yield pairs of pure-state single photons. One approach is to choose a set of operating wave-

#182231 - $15.00 USD Received 21 Dec 2012; revised 21 Feb 2013; accepted 21 Feb 2013; published 1 Mar 2013

lengths with zero group-velocity mismatch under what are termed extended phase-matching conditions [29, 30, 32]. In this regime and under pulsed pumping with a matching bandwidth, the joint spectral density is nearly circularly symmetric, giving rise to a biphoton state that has a low degree of spectral correlation and hence a high level of spectral purity for heralded single photons. Another approach, which also leads to spectral decorrelation, operates in a regime wherein the spectral widths for the two SPDC photons are highly asymmetric, with their joint spectral density resembling a highly-eccentric ellipse [33]. Both symmetric [18, 22] and asymmetric [13] group-velocity matching have been demonstrated, showing these methods to be good approaches for generating spectrally-decorrelated biphotons. Other techniques include SPDC in microstructured fibers [19], use of counter-propagating SPDC [34], and use of an external cavity [23, 35].

In the symmetric group-velocity matching case, it was found that the spectral purity was limited by the side lobes of the standard phase-matching function's $\mathrm{sinc}(\cdot) \equiv \sin(\cdot)/(\cdot)$ form, and that a Gaussian-shaped phase-matching function would in principle create full spectral decorrelation [18]. It is therefore desirable to modify the grating structure of periodically-poled materials such as PPKTP to obtain a Gaussian-shaped phase-matching function. Recently, Brańczyk *et al.* showed that by varying the poling-order of PPKTP with near 50:50 duty cycles, it was possible to modulate the effective optical nonlinearity to produce an approximately Gaussian phase-matching function [21].

In this work we report a different approach to obtain a Gaussian phase-matching function by varying the duty cycle of each poling period along the length of a first-order grating in a PPKTP crystal. By keeping its poling period fixed, we maintain better control over the phase-matching bandwidth and operating wavelengths. Additionally, we obtain a higher effective nonlinearity because first-order poling is used throughout the crystal. We demonstrate the method in a custom-designed PPKTP crystal in the extended phase-matching regime by mapping out the phase-matching function through difference-frequency generation (DFG) measurements, and analyze the effectiveness of our custom-made PPKTP crystal as a source of heralded pure-state single photons for quantum information science applications.

2. Grating structure modification

Efficient three-wave mixing in nonlinear crystals relies on phase matching to yield substantial nonlinear outputs (see Refs. [36] and [37]). For a non-depleting input pump E_1 with a fixed frequency ω_1 and a tunable input probe E_2 with frequency ω_2, the standard coupled-mode equations yield

$$E_3 = \Gamma d_{\mathrm{eff}} L G(\Delta k)\,, \tag{1}$$

for the output signal field E_3 with frequency ω_3. Here: d_{eff} is the effective nonlinear coefficient; L is the crystal length; $\Gamma = -i\omega_3 E_1 E_2^* / n_3 c$; c is the speed of light in vacuum; n_j is the crystal's index of refraction for the E_j field with $j = \{1,2,3\}$; Δk is the longitudinal wave-vector mismatch in the nonlinear material; and $G(\Delta k)$ is the phase-matching function given by

$$G(\Delta k) = \frac{1}{L}\int_0^L g(z)\exp(-i\Delta k z)dz, \tag{2}$$

$$\Delta k = k_1 - k_2 - k_3, \tag{3}$$

with $g(z) = d(z)/d_{\mathrm{eff}}$ being the signed fractional nonlinear coefficient whose value is bounded by ± 1, and k_j the wave-vector inside the crystal for the E_j field with $j = \{1,2,3\}$. For standard quasi-phase matching $g(z)$ is $+1$ for one polarization of the ferroelectric domains and -1 for the opposite polarization. To maximize efficiency the ideal first-order grating structure is composed of alternating equal-length segments of $g(z) = 1$ and $g(z) = -1$. Each segment length is $\Lambda/2$, where Λ is the grating period, in which case the grating has a 50:50 duty cycle.

#182231 - $15.00 USD Received 21 Dec 2012; revised 21 Feb 2013; accepted 21 Feb 2013; published 1 Mar 2013

The output intensity for this type of interaction is given by:

$$I_3 = \frac{1}{2} n_3 c \varepsilon_0 |E_3|^2 = \alpha |G(\Delta k)|^2 \tag{4}$$

where

$$\alpha = \frac{8\pi d_{\text{eff}}^2 L^2 I_1 I_2}{c\varepsilon_0 n_1 n_2 n_3 \lambda_3^2}, \tag{5}$$

and ε_0 is the vacuum permittivity. Under conventional phase matching ($\Lambda \to \infty$), $g(z) = 1$ and $|G(\Delta k)|^2 = \text{sinc}^2(\Delta k L/2)$ yields the usual sinc-squared output as a function of the probe and signal wavelengths. The grating structure for quasi-phase matching allows the operating wavelengths to be tuned within the crystal's transparency window by adjusting the grating period Λ and the reduced output is given by $|G(\Delta k)|^2 = (4/\pi^2)\text{sinc}^2(\Delta k L/2)$.

It is clear from Eq. (2) that $G(\Delta k)$ and $g(z)$ are a Fourier transform pair and that the phase-matching function $G(\Delta k)$ can be tailored by modifying the grating structure $g(z)$ [37]. An example in nonlinear optics is to chirp the grating period for simultaneous second-harmonic generation and pulse compression [38]. A chirped grating has also been used to generate ultra-broadband biphotons via SPDC [39].

To generate a Gaussian phase-matching function should, in principle, be quite simple because the Fourier transform of a Gaussian is also a Gaussian, suggesting that we only need to use a Gaussian grating function $g(z)$. However, $d(z)$ is not a continuously variable function because the nonlinearity d_{eff} is fixed and the domain segments are fully aligned one way or the other so that $g(z)$ must be either $+1$ or -1. Moreover, poling limitations restrict domain-inversion periods to no shorter than a few microns. Therefore, in practice, $g(z)$ is designed with numerical modeling and evaluation. Given that $g(z)$ is constant within each ferroelectric domain segment and that it changes sign across the poling boundary, one can write the spatial nonlinearity function as

$$g(z) = \sum_{j=0}^{N} (-1)^j \left[H(z - z_j) - H(z - z_{j+1}) \right], \tag{6}$$

where $H(z)$ is the unit step function and z_j is the j-th poling boundary, N is the number of domain segments, with $z_0 = 0$ and $z_{N+1} = L$. The mismatch function can then be evaluated with the result being

$$G(\Delta k) = \frac{2}{\Delta k L} \sum_{j=0}^{N} (-1)^j \sin[\Delta k (z_{j+1} - z_j)/2] \exp[-i \Delta k (z_{j+1} + z_j)/2]. \tag{7}$$

Equation (7) yields the desired grating period $\Lambda \equiv 2(z_{j+1} - z_j) = 2\pi/\Delta k_c$ for standard quasi-phase matching with equal domain segment lengths, where Δk_c is the wave-vector mismatch at the center operating wavelengths. For example, in type-II phase-matched SPDC with degenerate output frequencies or DFG with a fixed pump frequency, we have $\Delta k_c = k_1(\omega_1, n_1) - k_2(\omega_1/2, n_2) - k_3(\omega_1/2, n_3)$, in which the probe and signal refractive indices, n_2 and n_3, can be different.

It is possible to recast Eq. (7) in a different form or approximate it to clarify features of interest, such as the usual sinc-function behavior or how period or duty-cycle deviations affect the efficiency [37]. Here we focus on how to generate an approximately Gaussian phase-matching function for $|G(\Delta k)|^2$ as the signal frequency is tuned. The relationship between Δk and the operating wavelengths (frequencies) can be found using the appropriate Sellmeier equations for the nonlinear medium [40–43], which together with Eq. (7) should allow us to perform numerical modeling and compare it with measured data.

#182231 - $15.00 USD Received 21 Dec 2012; revised 21 Feb 2013; accepted 21 Feb 2013; published 1 Mar 2013

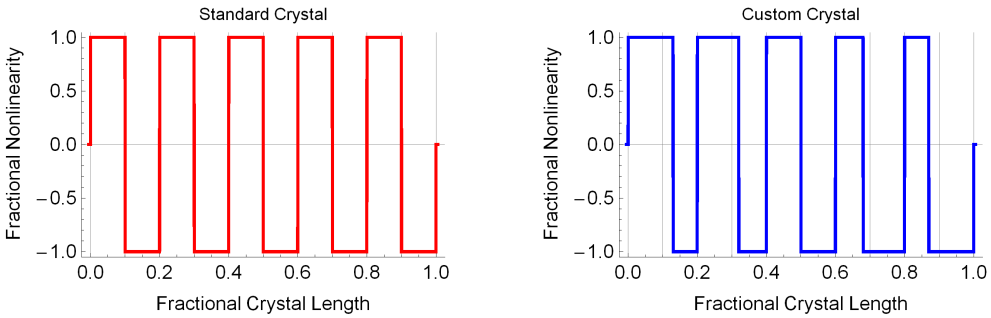

Fig. 1. Illustration of 50:50 duty cycle (left panel) and modulated duty cycle (right panel). Both cases have the same poling period, but the ratio of positive to negative domain segments changes along the length of the crystal when duty-cycle modulation is employed.

Equation (7) clearly indicates that the tool for modifying $G(\Delta k)$ is to manipulate the poling boundaries $\{z_n\}$. In Ref. [21] this was done by varying the grating period along the crystal. We opt for the different strategy of modifying the poling duty cycle (the ratio of positive to negative poling segments) with a single fixed grating period, something that we believe may be easier to implement and may lead to more efficient biphoton generation. In our approach the spacing $z_{2(j+1)} - z_{2j}$ between even-numbered boundaries is held constant at the grating period $\Lambda = 2\pi/\Delta k_c$, while the odd-numbered boundaries take the form $z_{2j+1} = (j + r_j)\Lambda$, with $0 < r_j < 1$ being the duty cycle. This duty-cycle variation method—illustrated conceptually in Fig. 1—affords a smooth modulation of the optical nonlinearity's effective strength.

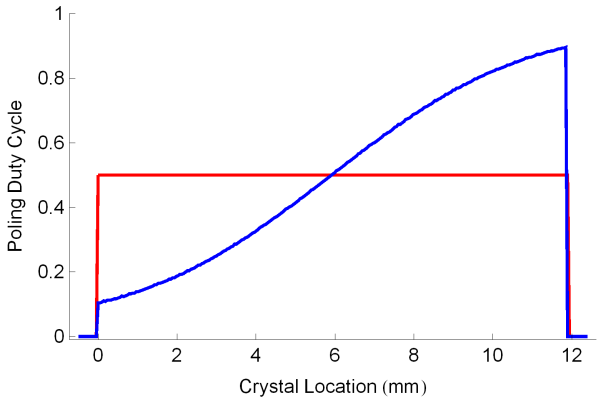

Fig. 2. Duty-cycle modulations for periodically-poled crystals. The blue curve shows the duty-cycle variation along the length of a custom-poled 12-mm-long PPKTP crystal, governed by Eq. (8). The red curve shows the duty cycle along the length of a uniformly poled, 50:50 duty-cycle PPKTP crystal of equivalent length.

Our goal is to create spectrally-factorizable biphoton states via type-II phase-matched SPDC—in which the two photons are spectrally indistinguishable and orthogonally polarized—that can be utilized to herald pure-state single photons. These desiderata can be achieved in PPKTP under extended phase-matching conditions at the degenerate output wavelengths of $\sim$1582 nm using a Gaussian-shaped phase-matching function [18, 30]. The required grating period Λ for this case is 46.1 μm.

#182231 - $15.00 USD Received 21 Dec 2012; revised 21 Feb 2013; accepted 21 Feb 2013; published 1 Mar 2013

For our crystal design we chose $\Lambda = 46.0\,\mu$m to allow for angle tuning, and a crystal length of $L = 12$ mm, resulting in about 520 domain segments. We worked with PPKTP manufacturer AdvR Inc. to implement our grating design within its manufacturing capability. In particular, poling domain segments shorter than about $5\,\mu$m are not advisable, because of domain fusing and poling irregularity. Using the Sellmeier equations in Ref. [43] we have developed a numerical model to predict the effects of different duty-cycle modulations. We start with a duty-cycle modulation that is nearly Gaussian: it is 50:50 at the center of the crystal $z = L/2$, and it decreases (increases) toward the beginning (end) of the crystal $z = 0$ ($z = L$). We use our numerical model to optimize and fine tune the characteristics of the resulting phase-matching function, especially in its side lobes because they give rise to undesirable asymmetry in the biphoton's joint spectral density. Figure 2 displays the final design for the 12-mm-long type-II quasi-phase-matched bulk KTP crystal and the duty-cycle $r(z)$ can be approximated by:

$$r(z) = \frac{1}{2}\left[1 + 0.9\,\mathrm{erf}\left(\frac{z - L/2}{0.45L}\right)\right] \approx 0.9 \times \exp\left[-\left(\frac{z - L}{0.655L}\right)^2\right]. \tag{8}$$

We obtain the discrete-domain duty cycles $\{r_j\}$ by evaluating $\{r(z_{2j})\}$ from Eq. (8) and rounding those values to the nearest $0.1\,\mu$m. The resulting model has a duty cycle of 10.2% at one end, and 89.8% at the other end. For a poling period of $46.0\,\mu$m this gives a minimum domain segment width of $4.7\,\mu$m, the constant offset and sub-unity magnitude of the error function in Eq. 8 are chosen to preclude domain segments shorter than this. The nearly Gaussian error-function modulation was chosen over a true Gaussian modulation to allow for a more straightforward optimization of the numerical model while incorporating manufacturing constraints. The design choice is expected to yield a nearly Gaussian phase-matching function. We note that the numerical model allows us to investigate the effects of angle tuning and possible crystal manufacturing defects such as over-poling, missed poling domains, and random boundary-location errors.

3. Experimental characterization

We characterized the custom-poled crystal's phase-matching function by DFG measurements. The type-II phase-matched PPKTP crystal was oriented horizontally (vertically) with respect to the crystal's *y*-axis (*z*-axis) with light propagation occurring along the crystal's *x*-axis. A horizontally-polarized pump beam at 790.9 nm was chopped at 600 Hz for lock-in detection and focused into the crystal with an average power of 150 mW at the crystal. A 2 mW, vertically-polarized probe beam was derived from a continuous-wave (cw) tunable laser operating at a 1582 nm center wavelength. The two beams were focused at the center of the crystal with a common focal parameter of $\zeta = L/b \approx 0.17$, where $b = 2\pi n_j w^2/\lambda_j$ is the confocal parameter, n_j is the crystal's refractive index at the vacuum wavelength λ_j, w_j is the beam waist, L is the crystal's length, and $j = \{1,2\}$ for pump and probe, respectively. The resulting DFG signal was horizontally polarized, centered at 1582 nm wavelength, and modulated by the 600 Hz chopping of the pump input. After the crystal, we blocked the pump and probe beams using a combination of spectral and polarization filters. The transmitted DFG signal output was coupled into a multi-mode optical fiber and detected with a low-noise InGaAs photodetector (Thorlabs model PDA-255). The output of the photodetector was sent to a lock-in amplifier that was synchronized to the pump-beam chopping frequency. We recorded the synchronously-detected DFG signal as a function of probe wavelength λ_2 between 1572 nm and 1592 nm, providing a direct measurement of $|G(\Delta k)|^2$ for a fixed pump wavelength $\lambda_1 = 790.9$ nm.

The measured $|G(\Delta k)|^2$ is very close to Gaussian—indicating the crystal has the desired characteristics—however, its bandwidth is 23% wider than expected. The measured DFG band-

#182231 - $15.00 USD Received 21 Dec 2012; revised 21 Feb 2013; accepted 21 Feb 2013; published 1 Mar 2013

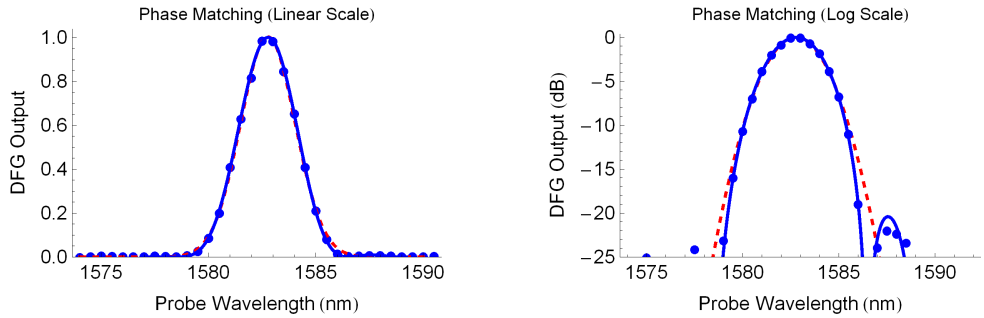

Fig. 3. The measured data, a Gaussian fit to the data, and the predicted DFG output (proportional to $|G(\Delta k)|^2$) of the custom-poled crystal are shown as a function of wavelength of the tunable probe laser λ_2 with the pump-laser wavelength fixed at 790.9 nm. Blue points show the measured data, the blue curve shows the predictions from the numerical crystal model of Eq. (7), the dashed red curve shows a Gaussian function fit to the measured data. The same data are plotted on linear (left panel), and dB (right panel) scales. Uncertainties in the measured data are approximately $\pm 3 \times 10^{-3}$ or -25 dB.

width, full width at half-maximum (FWHM), is 3.1 nm compared with the predicted DFG bandwidth of 2.5 nm, indicating that although the crystal exhibits a Gaussian shaped phase-matching function, there are manufacturing errors such as missed or partially-inverted domains.

We modeled the effect of missed small domain segments—where all domain segments below a certain size were missed, hence rendering that period to be unpoled. The main effect of this defect was a shorter effective crystal length and therefore a widening of the phase-matching function. Indeed, the phase-matching function only began to be distorted in other ways (the presence of an additional small side lobe, comparable in size to the one predicted for an ideal custom poled crystal) if all domain segments below 9.4 μm were missed, leaving a crystal with a duty cycle range of 20.4% to 79.6%. However, it only takes missed domain segments below 7.0 μm (15.2% to 84.8% duty cycle range) to account for the observed 3.1 nm phase-matching bandwidth. This type of defect is not entirely unexpected, indeed, even for crystals with uniform grating periods that are large compared to our smallest domain segment, errors in phase-matching width of 3 to 4 percent are present [31].

In Fig. 3 we compare the DFG measurements (blue points) with its Gaussian fit (dashed red curve) and the DFG response $|G(\Delta k)|^2$ predicted by our numerical model (blue curve) after scaling to match the experimentally-observed bandwidth. We plot the data on a linear scale (left panel), as well as on a logarithmic scale (right panel) to better show the fine details in the wings of the phase-matching function. The measured data agree well with predictions for the central Gaussian region, the small residual lobe near 1588 nm, and there being no other wavelengths with appreciable DFG output. The Gaussian fit closely follows the measured data, with significant deviations only occurring below -15 dB.

Although the measured DFG interaction is centered slightly away from the center of the extended phase-matching condition, the combination of temperature and angle tuning the crystal allow us to shift the DFG interaction's center wavelength. Moreover, this tuning does not impair the crystal's performance, because these tuning techniques only shift the phase-matching function as a whole; they do not modify its Gaussian shape.

#182231 - $15.00 USD Received 21 Dec 2012; revised 21 Feb 2013; accepted 21 Feb 2013; published 1 Mar 2013

4. Implications for quantum information science

The custom-poled PPKTP crystal can be used to generate spectrally unentangled two-photon states from which the heralded pure-state single-mode photons that are essential for many quantum information science applications can be obtained. In this section we evaluate numerically the expected single-mode purity of heralded single photons based on the custom-designed PPKTP crystal whose phase-matching function is well approximated by our Eq. (7) model, as shown in Fig. 3. In quantum-mechanical terms, the SPDC process involves absorbing a pump photon at ∼791 nm and converting it to two subharmonic photons—called signal (s) and idler (*i*)—at ∼1582 nm. For type-II phase-matching in PPKTP the signal and idler photons are orthogonally polarized, which allows easy separation by a polarization beam-splitter. The quantum state of this biphoton is determined by the frequency spectrum of the pump field $E_p(\omega)$ and the phase-matching function of the crystal $G(\Delta k)$. Neglecting inconsequential normalization constants and assuming collinear plane-wave propagation (i.e., loose pump focusing), the SPDC biphoton state is given by [32]:

$$|\psi\rangle = \int \frac{d\omega_s}{2\pi}\frac{d\omega_i}{2\pi}\beta(\omega_s,\omega_i)G(\Delta k)\,|\omega_s\rangle|\omega_i\rangle\,, \tag{9}$$

where

$$\beta(\omega_s,\omega_i) = \frac{\sqrt{\omega_s\omega_i}}{n_s n_i}E_p(\omega_s+\omega_i)\,, \tag{10}$$

$|\omega_s\rangle$ ($|\omega_i\rangle$) is a single-photon state with signal (idler) frequency ω_s (ω_i), and the pump's intensity spectrum $|E_p|^2$ is centered at ω_p with bandwidth Ω_p. Alternatively, we can express the state in terms of vacuum wavelengths:

$$|\psi\rangle = \int d\lambda_s d\lambda_i \tilde{\beta}(\lambda_s,\lambda_i)G(\Delta k)\,|\lambda_s\rangle|\lambda_i\rangle\,, \tag{11}$$

where

$$\tilde{\beta}(\lambda_s,\lambda_i) = \frac{1}{(\lambda_s\lambda_i)^2}\times\beta\left(\frac{2\pi c}{\lambda_s},\frac{2\pi c}{\lambda_i}\right), \tag{12}$$

and we have again neglected a normalization constant.

We analyze our crystal's performance using two metrics: the entropy of entanglement H_ψ [44] and the heralded-state purity P_ψ [33]. A Schmidt decomposition [27] on the biphoton quantum state results in a set of Schmidt coefficients $\{k_i\}$. The entropy of entanglement measures shared information between the signal and idler photons, and is defined as the Shannon entropy of these Schmidt coefficients:

$$H_\psi \equiv -\sum_i k_i \log_2 k_i, \tag{13}$$

where the base-2 logarithm implies that the units of H_ψ are bits. The heralded-state purity measures the purity of the signal (idler) single-photon state when the presence of the idler (signal) photon is used for heralding. Mathematically, this purity is defined as the normalized sum of the squared Schmidt-coefficients (equivalent to the inverse of the Schmidt number):

$$P_\psi \equiv \left(\sum_i k_i^2\right)\Big/\left(\sum_i k_i\right)^2. \tag{14}$$

To quantify the benefits of the Gaussian phase-matching function, we compare our custom-poled crystal with a standard crystal for frequency-degenerate, type-II phase-matched SPDC

#182231 - $15.00 USD Received 21 Dec 2012; revised 21 Feb 2013; accepted 21 Feb 2013; published 1 Mar 2013

outputs centered at 1582 nm using a pulsed pump centered at 791 nm. We employ our numerical model from Eq. (7) to approximate $G(\Delta k)$ of our 12-mm-long PPKTP crystal with its modulated duty cycle, and include a wavelength scaling to match the observed phase-matching bandwidth that is ∼23% wider than expected. This amounts to assuming that $G(\Delta k)$ has no extraneous phase behavior unaccounted for in Eq. (7). For comparison, we assume the usual sinc-function phase matching for an 8.1-mm-long PPKTP crystal, in which the crystal length is chosen to match the observed phase-matching bandwidth of the custom-poled crystal. Figure 4 shows the two performance metrics H_ψ (left panel) and P_ψ (right panel) for the standard uniformly-poled crystal (red curve) and custom-poled crystal (blue curve) as a function of the full-width at half-maximum (FWHM) bandwidth $\Delta\lambda_p$ of the pump's Gaussian-shaped intensity spectrum. For all evaluated values of the pump bandwidth the custom-poled crystal shows improved results compared with those obtained with the standard crystal. The standard uniformly-poled crystal with a 1.30 nm FWHM pump bandwidth produces a biphoton state with a minimum entropy of entanglement of 0.71 bits, corresponding to a maximum heralded state purity of ∼83%, whereas pumping our custom-poled crystal with a 1.40 nm bandwidth yields a state with a minimum entropy of entanglement of 0.16 bits and a corresponding heralded-state purity of 97%.

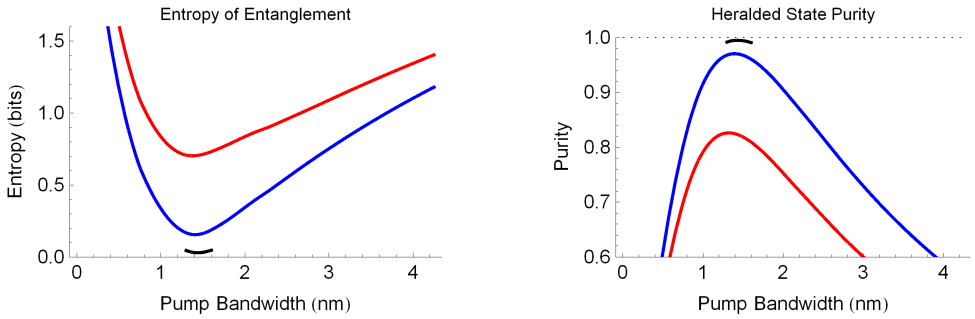

Fig. 4. Entropy of entanglement H_ψ from Eq. (13) (left panel) and heralded-state purity P_ψ from Eq. (14) (right panel) as functions of FWHM pump bandwidth. The red curves show the results for the output state of a 8.1 mm long standard uniformly-poled PPKTP crystal, and the blue curves display the results for the output of our custom Gaussian duty-cycle modulated 12 mm long crystal. The black curves near the optimal pump bandwidth of 1.40 nm show the results for the output of our custom-poled crystal with mild filtering (8.5 nm FWHM filter). The dotted line on the purity plot at $P_\psi = 1$ is the maximum possible purity.

The dramatic improvement in heralded-state purity with the use of a near-Gaussian phase-matching profile is obtained without spectral filtering. However, it is possible to increase the purity even further by mild spectral-filtering the output state, which entails only modest flux loss. Figure 4 plots the results of applying a 8.5 nm FWHM Gaussian spectral filter to both the signal and idler outputs (black curves) when using the optimal 1.40 nm pump bandwidth; this spectral-filter bandwidth is more than twice the SPDC output bandwidth. The spectrally-filtered heralded-state purity P_ψ reaches 99.5% at the expense of 10% filtering transmission loss for each beam (assuming unity peak-transmission efficiency for the filters). This capability gives flexibility to further fine tune the output state characteristics, however an important point to note is that this filtering will reduce the total flux as well as the heralding efficiency [26].

Figure 5 displays the calculated joint spectral amplitude $|\tilde{\beta}(\lambda_s,\lambda_i)G(\Delta k)|$ for the minimum-entropy biphoton states obtained for the standard uniformly-poled 8.1-mm crystal (left panel) with 1.30 nm pump bandwidth and the custom-poled 12-mm crystal (right panel) with 1.40 nm

#182231 - $15.00 USD Received 21 Dec 2012; revised 21 Feb 2013; accepted 21 Feb 2013; published 1 Mar 2013

pump bandwidth. Both states have nearly circular central lobes. However the side lobes, clearly present in the standard crystal's output, are strongly suppressed in our custom-poled crystal's output, as expected from its increased purity. The effect of a mild spectral filter, not shown in Fig. 5, is to further reduce the residual side lobes for the custom-poled source enabling its output to achieve even higher purity.

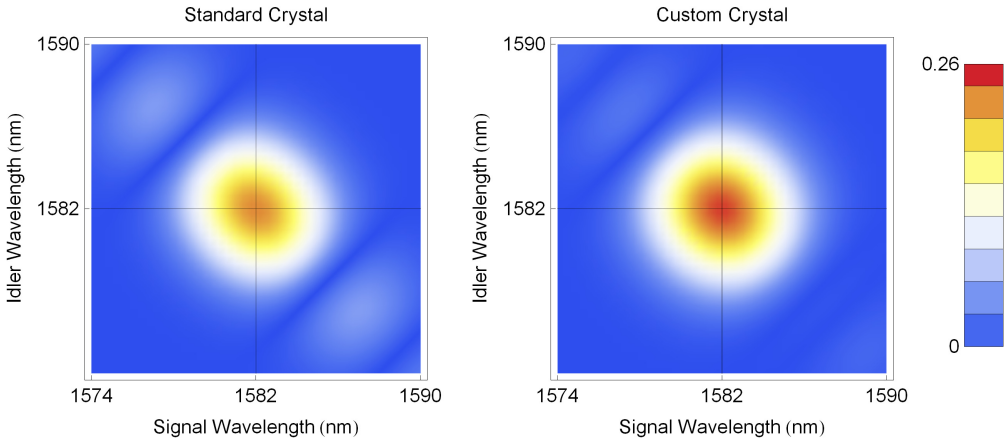

Fig. 5. Calculated joint spectral amplitudes $|\tilde{\beta}(\lambda_s,\lambda_i)G(\Delta k)|$ are shown in density plots for SPDC output states from a standard uniformly-poled 8.1 mm crystal (left panel) and for our Gaussian duty-cycle modulated 12 mm crystal (right panel). Side lobes are strongly suppressed in the state from the Gaussian duty-cycle modulated crystal. The legend on the right is in units of nm^{-2}.

It can be informative to compare the characteristics of several different crystal types of the same crystal length. We consider the following PPKTP crystals with 12 mm length: a standard crystal with uniform poling, a previously demonstrated crystal with poling-order modulation [21], our custom crystal model with duty-cycle modulation, and finally our custom crystal incorporating a 8.5 nm (FWHM) spectral filter on the output. When comparing these crystals, characteristics of interest include general properties of the crystal itself, as well as the two performance metrics of the SPDC output state using their respective optimal pump bandwidths that maximize heralded-state purity with the same total pump power.

Table 1 shows our numerical evaluation of four different crystal types (with the same 12-mm crystal length). The second column shows their relative nonlinearity strength, defined as the maximum DFG field strength for each crystal relative to that of a standard crystal, indicating that our use of a fixed period, first-order grating with variable duty cycles is more efficient than the adding of higher poling-orders used in [21]. The DFG phase-matching bandwidth (FWHM) for a monochromatic pump is also evaluated, showing that our crystal has a narrower bandwidth than that in [21]. Note also that the effective bandwidth is slightly narrower when mild spectral filtering is included with our crystal. Of particular interest to quantum information processing are the maximum heralded-state purity P_ψ and the minimum entropy of entanglement H_ψ. Also of interest are the relative SPDC output flux, defined as $\int\int|\tilde{\beta}(\lambda_s,\lambda_i)G(\Delta k)|^2 d\lambda_s d\lambda_i$ for each crystal relative to that of a standard crystal, and the output SPDC FWHM bandwidth. The two methods of generating Gaussian phase-matching functions used by [21] and in this work yield similar minimum entropy and single-mode purity of $\sim$97%, with the flux associated with duty-cycle modulation being $>$50% higher than that of poling-period modification. Both types of modulated crystals yield much higher purity than a standard uniformly-poled crystal at the

#182231 - $15.00 USD Received 21 Dec 2012; revised 21 Feb 2013; accepted 21 Feb 2013; published 1 Mar 2013

expense of reducing the total flux. Adding spectral filtering with an 8.5 nm bandwidth to the outputs of the duty-cycle modulated crystal is expected to yield a purity of 99.5%, yet the flux is only reduced by 20%. Similar spectral filtering can be applied to the variable poling case of [21]—adding spectral filtering with an 11.3 nm bandwidth (matched to reduce flux by 20%) to the outputs of this crystal is expected to yield a purity of 99.8%. Note that our duty-cycle modulated crystal is limited by the ability to manufacture narrow domain segments, whereas the crystal of Brańczyk *et al.* does not have this limitation.

Table 1. Calculated output characteristics of five different PPKTP crystal types (12-mm crystal length): standard uniformly-poled crystal (Standard), poling-order modulated crystal of Brańczyk *et al.* [21] (Poling-Order), the crystal of Brańczyk *et al.* with 11.3 nm wide spectral filtering of the SPDC output (Poling-Order Filtered), our custom duty-cycle modulated crystal (Duty-Cycle), our our custom duty-cycle modulated crystal with 8.5 nm wide spectral filtering of the SPDC output (Duty-Cycle Filtered). Calculated characteristics are: nonlinearity strength relative to the standard crystal (Rel. NL), output DFG FWHM spectral bandwidth for a monochromatic pump (DFG BW), maximum heralded-state purity (Purity), the minimum state-entropy (Entropy), SPDC output flux relative to the standard crystal (Flux), and SPDC FWHM bandwidth (SPDC BW).

Crystal type	Rel. NL	DFG BW	Purity	Entropy	Flux	SPDC BW
Standard	1.00	2.09 nm	81.8%	0.76 bits	1.00	2.70 nm
Poling-Order	0.45	3.45 nm	97.4%	0.13 bits	0.34	5.16 nm
Poling-Order Filtered	0.45	3.30 nm	99.8%	0.01 bits	0.27	4.67 nm
Duty-Cycle	0.62	3.08 nm	97.0%	0.16 bits	0.53	4.05 nm
Duty-Cycle Filtered	0.62	2.90 nm	99.5%	0.03 bits	0.43	3.67 nm

5. Conclusions

We have demonstrated a method for engineering a nearly Gaussian phase-matching function of PPKTP by smoothly modulating the duty cycle of the grating structure with a fixed grating period. We verified the phase-matching characteristics using optical difference-frequency generation and found them to be in good agreement with our numerical calculations. Under extended phase-matching conditions the custom-poled PPKTP crystal should enable the generation of spectrally factorizable biphotons via pulsed SPDC with an appropriately selected pump bandwidth. We expect our duty-cycle modulated PPKTP to yield heralded single photons with single-mode purity of $\sim$97%, and may reach as high as 99.5% if mild spectral filtering is used to suppress residual side lobes. This type of engineered SPDC source with outputs of high-purity single photons is very well suited for applications requiring multi-photon or cascaded HOM-type quantum interactions between photons. We expect it to be part of a growing quantum information processing toolbox for use in a variety of quantum measurement applications.

Acknowledgments

This work was sponsored by the Office of the Assistant Secretary of Defense for Research and Engineering.

#182231 - $15.00 USD Received 21 Dec 2012; revised 21 Feb 2013; accepted 21 Feb 2013; published 1 Mar 2013